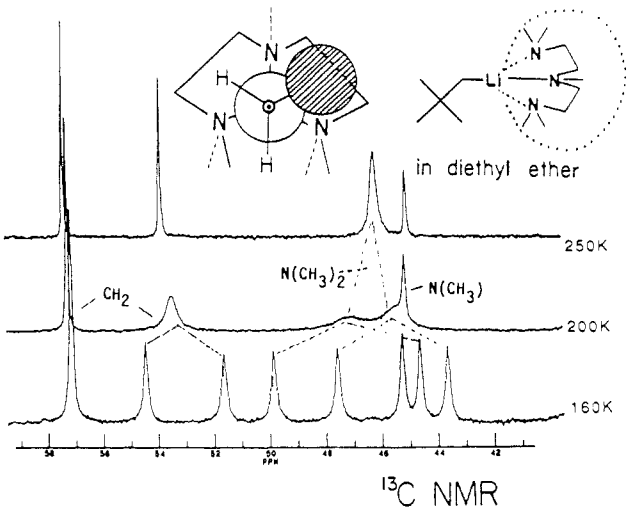

Figure 1. ^{13}C NMR, 75 MHz, ligand resonances of [^{6}Li]neopentyllithium M, in diethyl ether containing 1 equiv of *N,N,N',N',N''*-pentamethyldiethylenetriamine, different temperatures. Temperature calibrated by method of Van Geet.[14,15]

amine moiety and both lithium and the NCH_3 nitrogen are chiral centers, see **2**. This conclusion is supported by the results of a

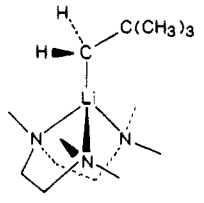

2

fully optimized structure of **1** complexed to PMDTA, using MNDO.[13] The complex is unsymmetrical with the C-methyls closer to one terminal nitrogen (N_1) than the other, thus by steric repulsion forcing the N_1–Li distance to exceed that of N_3 to Li. Inspection of the model reveals minimum steric interactions between the *tert*-butyl methyls and the *N*-methyls compared to the other rotamers.

The NMR data for **1**·PMDTA at 146 K show inversion at nitrogen to be slow relative to the NMR time scale as is also rotation about the CH_2–Li axis and Li–N coordination exchange.

Further assignments of ^{13}C shifts in **1**·PMDTA and insight into dynamic effects come from NMR behavior observed above 146 K. With increasing temperature there is signal averaging which involves all the ^{13}C PMDTA resonances except the one at 45.38 δ, which must be due to N_2–CH_3. This assigns the peaks at 43.78, 44.75, 47.69, and 49.98 δ, respectively, to $N(CH_3)_2$ carbons, Figure 1. Between 166 and 216 K three pairs of resonances—all δ units, CH_2 at 54.58 and 51.74, $N(CH_3)_2$ methyls at 43.77 and 47.69 and a second pair at 44.76 and 49.97—each average to broad lines at their respective centers, Figure 1. NMR line shape analysis shows the process responsible for this low-temperature signal averaging is the same for all three collapsing doublets. But since the methylene doublet must come from CH_2's at opposite ends of the ligand, then the averaging mechanism is rotation about the CH_2–Li axis. In that case one can classify the $N(CH_3)_2$ resonances as 43.77 δ and 47.69 δ on one side and equidistant to Li and 44.76 δ and 49.97 δ on the other side.

A second dynamic process is seen in the ^{13}C NMR of **1**·PMDTA above 200 K, the averaging of all the ^{13}C $N(CH_3)_2$ resonances. We would like to propose this is the result of reversible N–Li coordination exchange, each dissociation being accompanied by one or more inversions. The process appears to be synchronous with the exchange of neopentyls and lithiums between monomer and dimer. For, above 200 K their respective ^{13}C and ^{6}Li resonances also signal average, and the rate constants derived from line shape analysis are closely similar to those for N–Li coordination exchange. We also observe qualitatively that the N–Li coordination exchange rate increases with the concentration of ether-solvated dimer. Taking account of both internal rotation about the CH_2–Li axis and N–Li coordination exchange in the ^{13}C NMR line shape analysis[9] of complexed PMDTA gives rise to $\Delta H_r^{\ddagger} = 7.7$ kcal and $\Delta S_r^{\ddagger} = -3.4$ eu for rotation and $\Delta H_e^{\ddagger} = 8.8$ kcal and $\Delta S_e^{\ddagger} = -8.3$ eu for the slower coordination exchange.

In sum we have been able to describe the structure of a chiral monomeric tridentately coordinated complex of **1** with PMDTA because at 160 K the species is conformationally locked into one rotamer, due to steric interactions, and all bond exchange processes (C, Li and N, Li) are slow relative to the NMR time scale. Then at higher temperatures a detailed dynamic picture of rotationand the just mentioned bond exchanges has been revealed by using our methods of NMR line shape analysis.

Acknowledgment. This research was supported by the National Science Foundation Grant No. CHE 8304636 and in part by the Goodyear Tire and Rubber Company. Purchase of high field NMR equipment was also financed in part by grants from the National Science Foundation. We thank Dr. Charles Cottrell, Central Campus Instrumentation Center, for technical consulting.

Supplementary Material Available: Coupled density matrix equations together with an exchange matrix, figures representing experimental and calculated line shapes and Eyring plots, and a table listing the shifts, line widths, and fitted rate constants (10 pages). Ordering information is given on any current masthead page.

(13) Dewar, M. J. S.; Thiel, W. *J. Am. Chem. Soc.* **1977**, *99*, 4399. Thiel, W.; Clark, T. Quantum Chemistry Program Exchange, Indiana University, 1983; 438.

(14) Van Geet, A. L. *Anal. Chem.* **1970**, *42*, 679.

(15) These samples did not precipitate or freeze down to the lowest temperatures used, 146 K.

Structure of the 3Fe–4S Cluster in *Desulfovibrio gigas* Ferredoxin II

Charles R. Kissinger,* Elinor T. Adman, Larry C. Sieker, and Lyle H. Jensen

Department of Biological Structure, SM-20
School of Medicine, University of Washington
Seattle, Washington 98195

Received August 22, 1988

Since the discovery of 3-Fe clusters in proteins,[1] their structure and composition have been controversial. Recently in our laboratory, the structure of ferredoxin I from *Azotobacter vinelandii* was redetermined at 2.6 Å resolution.[2] It was demonstrated that the first reported structure[3] for this protein was in error and that the 3-Fe cluster in the molecule appears to be a 3Fe–4S cluster with a configuration much like the 4Fe–4S cubane-type clusters previously found in other proteins[4] but simply lacking one iron

(1) (a) Emptage, M. H.; Kent, T. A.; Huynh, B. H.; Rawlings, J.; Orme-Johnson, W. H.; Münck, E. *J. Biol. Chem.* **1980**, *255*, 1793–1796. (b) Huynh, B. H.; Moura, J. J. G.; Moura, I.; Kent, T. A.; LeGall, J.; Xavier, A. V.; Münck, E. *J. Biol. Chem.* **1980**, *255*, 3242–3244.

(2) Stout, G. H.; Turley, S.; Sieker, L. C.; Jensen, L. H. *Proc. Natl. Acad. Sci. U.S.A.* **1988**, *85*, 1020–1022.

(3) (a) Stout, C. D.; Ghosh, D.; Patthabi, B.; Robbins, A. H. *J. Biol. Chem.* **1980**, *255*, 1797–1800. (b) Ghosh, D.; O'Donnell, S.; Furey, W., Jr.; Robbins, A. H.; Stout, C. D. *J. Mol. Biol.* **1982**, *158*, 73–109. (c) A reanalysis of this work subsequent to ref 2 has been published (Stout, C. D. *J. Biol. Chem.* **1988**, *263*, 9256–9260).

(4) (a) Carter, C. W., Jr. In *Iron–Sulfur Proteins*; Lovenberg, W., Ed.; Academic Press: New York, 1977; Vol. 3, pp 157–204. (b) Adman, E. T.; Sieker, L. C.; Jensen, L. H. *J. Biol. Chem.* **1973**, *248*, 3987–3996. (c) Fukuyama, K.; Nagahara, Y.; Tsukihara, T.; Katsube, Y.; Hase, T.; Matsubara, H. *J. Mol. Biol.* **1988**, *199*, 183–193.

0002-7863/88/1510-8721$01.50/0

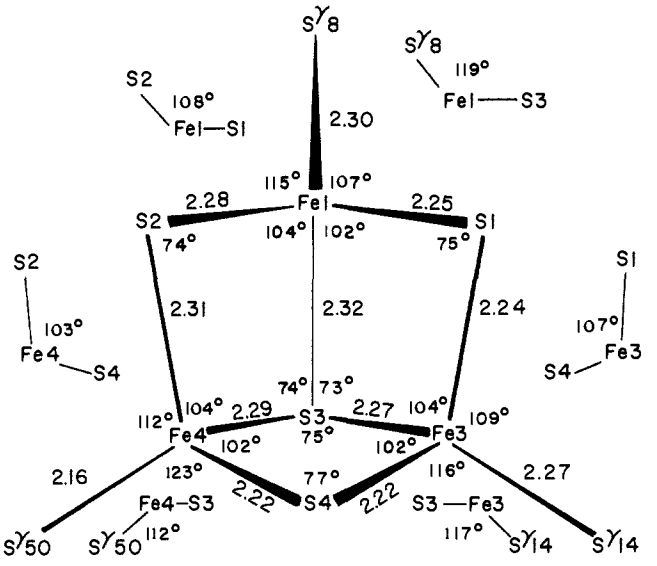

Figure 1. $Fe_3S_4S^{\gamma}_3$ complex in *D. gigas* ferredoxin II. The numbering of Fe and inorganic S atoms corresponds to that of equivalent atoms of *P. aerogenes* ferredoxin complex **1**.[4b] The number of S^{γ} atoms refers to the sequence position of the cysteine residue.

atom and a fourth cysteine ligand. We have now determined and refined the crystal structure of a second protein containing a 3-Fe cluster, ferredoxin II from *Desulfovibrio gigas*, at 1.7 Å resolution. This resolution is sufficient to resolve individual iron and sulfur atoms of the single 3-Fe cluster in the molecule and to refine the positions of these atoms without restraints. We describe here the structure of this cluster, which is a 3Fe–4S cluster with three cysteine ligands and geometry implying three equivalent iron atoms.

Ferredoxin from *D. gigas* is unusual in that the protein exists in two forms, with different Fe–S clusters bound by the same polypeptide chain.[5] Ferredoxin I is a dimer[6] of the ~6000 molecular weight ferredoxin monomer and contains one 4Fe–4S cluster per subunit, while ferredoxin II is a tetramer containing one 3Fe–4S cluster per subunit. The two forms can be interconverted reversibly.[7]

D. gigas ferredoxin II in oxidized form was crystallized as a monomer at pH 5.0,[8] and diffraction data to 1.7 Å were collected.[9] The structure was solved by the resolved anomalous phasing technique,[10] by using the positions of the iron atoms determined from an anomalous difference Patterson map. As is common for refinement of protein structures, a restrained-parameter least-squares refinement procedure[11] was used. No restraints, however, were imposed on distances or angles within the cluster. The crystallographic R factor is 0.176 for 4508 reflections ($F > 2\sigma_F$) between 8 and 1.7 Å resolution. The rms deviations from ideality in bond lengths and angles are 0.016 Å and 1.9°, respectively. Forty-four solvent molecules are included in the model. Full details of the structure determination and final molecular model will be described elsewhere.[12]

Table I. Equivalent Bond Lengths and Angles in the $Fe_3S_4S^{\gamma}_3$ Complex of *D. gigas* Ferrodoxin (DgFdII) and the $Fe_4S_4S^{\gamma}_4$ Complexes of *Chromatium vinosum* High-Potential Iron Protein (HiPIP) and *P. aerogenes* Ferredoxin (PaFd)

		DgFdII	HiPIP[a]	PaFd[b]
		Bond Lengths (Å)		
Fe···Fe	mean	2.75	2.72	2.73
	range	2.72–2.77	2.68–2.78	2.66–2.83
	rms dev	0.02	0.04	0.06
Fe–S	mean	2.27	2.26	2.25
	range	2.22–2.32	2.10–2.39	2.09–2.40
	rms dev	0.04	0.08	0.10
Fe–S^{γ}	mean	2.24	2.20	2.22
	range	2.16–2.30	2.17–2.22	1.98–2.43
	rms dev	0.06	0.02	0.16
		Bond Angles (deg)		
Fe–S–Fe	mean	74	74	75
	range	73–77	72–76	71–81
	rms dev	1.2	1.3	2.6
S–Fe–S	mean	104	104	103
	range	103–107	101–109	99–108
	rms dev	2.0	2.4	3.5
S^{γ}–Fe–S	mean	114	115	115
	range	107–123	107–120	101–127
	rms dev	4.7	4.9	8.0

[a] Reference 4a. [b] Reference 17.

Figure 1 depicts the 3-Fe complex (the cluster plus the three cysteine S^{γ} ligands) including values of individual bond lengths and angles. As shown in Table I, average values of bond lengths, bond angles, and Fe···Fe distances in the 3-Fe complex are remarkably close to those in the 4-Fe complexes of *Chromatium vinosum* high-potential iron protein and *Peptococcus aerogenes* ferredoxin. Indeed, none of the average values for corresponding bonds in the three structures differ significantly.[13]

The three divalent inorganic sulfur atoms and two of the cysteine S^{γ} atoms in the complex are involved in apparent NH···S hydrogen bonds with main-chain amide nitrogen atoms of the protein, as has been found for sulfur atoms of 4Fe–4S complexes in proteins,[14,4c] The single trivalent sulfur in the cluster is not hydrogen-bonded and is located in a nonpolar environment.

The model for the 3-Fe cluster described here is consistent with numerous spectroscopic and other studies[15] of proteins containing 3-Fe clusters. The 3Fe–4S clusters in *A. vinelandii* ferredoxin I and *D. gigas* ferredoxin II appear to be of the same type, although differences in resolution and state of refinement preclude any meaningful comparison of geometries. Despite this apparent structural similarity, there is a large difference in reduction potentials reported for the 3-Fe clusters in the two molecules (−420 mV for *A. vinelandii* ferredoxin I and −130 mV for *D. gigas* ferredoxin II[16]). The reasons for this remain to be determined.

(5) Bruschi, M.; Hatchikian, E. C.; LeGall, J.; Moura, J. J. G.; Xavier, A. V. *Biochim. Biophys. Acta* **1976**, *449*, 275–284.
(6) Although originally reported as a trimer (ref 5), ferredoxin I appears instead to be a dimer (Moura, J. J. G.; Moura, I. Personal communication).
(7) Moura, J. J. G.; Moura, I.; Kent, T. A.; Lipscomb, J. D.; Huynh, B. H.; LeGall, J.; Xavier, A. V.; Münck, E. *J. Biol. Chem.* **1982**, *257*, 6259–6267.
(8) Sieker, L. C.; Adman, E. T.; Jensen, L. H.; LeGall, J. *J. Mol. Biol.* **1984**, *179*, 151–155.
(9) The data set of 5180 Friedel pairs, comprising ~94% of the possible reflections of 1.7 Å, was obtained by using a Krisel Control-modified Picker four-circle diffractometer.
(10) (a) Hendrickson, W. A.; Teeter, M. M. *Nature (London)* **1981**, *290*, 107–113. (b) Hendrickson, W. A. *Acta Crystallogr., Sect. B* **1971**, *27*, 1474–1475.
(11) Hendrickson, W. A.; Konnert, J. H. In *Computing in Crystallography*; Diamond, R., Ramaseshan, S., Venkatesan, K., Eds.; Indian Academy of Science, International Union of Crystallography, Bangalore, 1980; pp 13.01–13.23.
(12) Kissinger, C. R.; Adman, E. T.; Sieker, L. C.; Jensen, L. H. Manuscript in preparation.
(13) Assuming the standard deviation in position of a S atom to be twice that of an Fe atom, we estimate $\sigma_{Fe} = 0.02$ Å and $\sigma_S = 0.04$ Å on the basis of the population variance of the 12 Fe–S bonds in the 3-Fe complex of *D. gigas* ferredoxin II. We note, however, that these bonds fall into three classes: Fe–S^{γ} bonds, Fe–S bonds involving divalent inorganic S atoms, and Fe–S bonds involving the single trivalent S atom. Although no significant differences in the average lengths of each kind of bond in the *D. gigas* complex are evident, the bond lengths may, in fact, differ. Therefore, the estimated σ_{Fe} and σ_S should represent upper bounds.
(14) (a) Carter, C. W., Jr.; Kraut, J.; Freer, S. T.; Alden, R. A. *J. Biol. Chem.* **1974**, *249*, 6339–6346. (b) Adman, E.; Watenpaugh, K. D.; Jensen, L. H. *Proc. Natl. Acad. Sci. U.S.A.* **1975**, *72*, 4854–4858.
(15) (a) Antonio, M. R.; Averill, B. A.; Moura, I.; Moura, J. J. G.; Orme-Johnson, W. H.; Teo, B. K.; Xavier, A. V. *J. Biol. Chem.* **1982**, *257*, 6646–6649. (b) Beinert, H.; Emptage, M. H.; Dreyer, J.-L.; Scott, R. A.; Hahn, J. E.; Hodgson, K. O.; Thomson, A. J. *Proc. Natl. Acad. Sci. U.S.A.* **1983**, *80*, 393–396. (c) Beinert, H.; Thomson, A. J. *Arch. Biochem. Biophys.* **1983**, *2*, 333–361. (d) Thomson, A. J.; Robinson, A. E.; Johnson, M. K.; Cammack, R.; Rao, K. K.; Hall, D. O. *Biochim. Biophys. Acta* **1981**, *637*, 423–432.
(16) (a) Sweeney, W. V.; Rabinowitz, J. C.; Yoch, D. C. *J. Biol. Chem.* **1975**, *250*, 7842–7847. (b) Cammack, R.; Rao, K. K.; Hall, D. O.; Moura, J. J. G.; Xavier, A. V.; Bruschi, M.; LeGall, J.; Deville, A.; Gayda, J. P. *Biochim. Biophys. Acta* **1977**, *490*, 311–321.

Acknowledgment. This work was supported in part by NIH Grants GM13366 and GM31770. We thank J. J. G. Moura, I. Moura, and J. LeGall for purified *D. gigas* ferredoxin II and S. Sheriff and B. Finzel for computer programs used in this work.

(17) Values are for complex 1 from data set 1FDX deposited with the Brookhaven Protein Data Bank (Berstein, F. C.; Koetzle, T. F.; Williams, G. J. B.; Meyer, E. F., Jr.; Brice, M. D.; Rodgers, J. R.; Kennard, O.; Shimanouchi, T.; Tasumi, M. *J. Mol. Biol.* **1977**, *112*, 535–542).

An Ionic System with Critical Point at 44 °C

Rajiv R. Singh and Kenneth S. Pitzer*

Department of Chemistry and Lawrence Berkeley Laboratory, University of California Berkeley, California 94720

Received August 1, 1988

Most ionic compounds have high melting points and exist as liquids only in solution in water or another solvent with high dielectric constant. Organic salts melting near 100 °C have been known, and their properties in solution have been investigated for many years.[1] Recently, Ford and his associates[2,3] prepared tetraalkylammonium tetraalkylborides that are liquid at room temperature and show high electrical conductance and other saltlike properties. We are interested in finding a model ionic system with phase separation and a critical point near room temperature. Our results may be of interest, however, in connection with other applications of liquid salts. The solubility properties of triethyl-*n*-hexylammonium triethyl-*n*-hexylboride ($N_{2226}B_{2226}$) were measured for several solvents, and an equation is presented which correlates the results. The system with diphenyl ether showed a critical point near 44 °C. Measurements of the coexistence curve are reported.

The salt $N_{2226}B_{2226}$ was synthesized by the procedure described by Ford and co-workers.[2] Atmospheric oxygen was carefully excluded. Although the product can be purified by liquid chromatographic separation on a silica gel column with 5% CH_3OH in CH_2Cl_2 as the solvent, it is preferable to carry out careful synthesis with purified reagents. The salt prepared by us had a pale yellow color indicating either an impurity or a low-lying absorption band. Previously, this compound has been reported to form only a glass on cooling, but we were able to crystallize it and observed a melting-point range of −22.5 to −21.7 °C. This indicates reasonably good purity, and it was not possible to separate the color from the salt by partial crystallization or liquid chromatography. This salt has been reported to be colorless;[1] hence, our sample may have had an impurity, but we believe the amount must have been very small.

The solubility of the salt in various solvents is expected to be influenced by two factors. The first relates to the ionic forces and is given by the principle of corresponding states as applied to ionic systems.[4] This implies increase of solubility with increase in dielectric constant ϵ. Also significant is the difference of Hildebrand's solubility parameters δ (the square root of the cohesive energy density): the larger the difference, the smaller the solubility. Thus, where the dielectric constant (or relative permittivity) of the solvent is greater than that given by the following expression for ϵ_m, we found large solubility and usually complete miscibility at room temperature:

$$\epsilon_m = [0.289 - 0.00316(\delta - 22.9)^2]^{-1} \quad (1)$$

Here δ is in $MPa^{1/2}$. Correspondingly, where ϵ for the solvent is less than ϵ_m, the solubility of salt in solvent was usually small and smaller where this difference was larger. For benzene, diphenyl ether, 1-bromooctane, and ethylene glycol, we observed substantial but limited solubility at room temperature. On moderate increase in temperature, diphenyl ether became miscible, whereas the solubility remained limited for the others. The full list of solvents tested is given below, and the one apparent exception is explained.

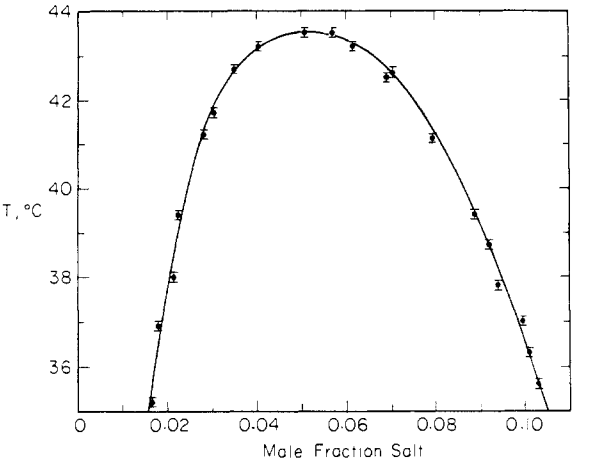

Figure 1. The phase boundary and critical point for the ionic system ($N_{2226}B_{2226}$ + diphenyl ether).

The coexistence curve was obtained with purified salt, and diphenyl ether was obtained as gold label grade from Aldrich Chemical. The desired amounts of each substance were added to glass ampoules, degassed, and then sealed. The phase separation was visually observed with the ampoules placed in a water bath controllable to ±0.01 °C. Strong critical opalescence was noticed in the near critical samples. The equilibrium was checked from both higher and lower temperatures. The sluggishness of the approach to equilibrium in the critical region of this viscous system precluded a match better than 0.08 °C betwen the two sets of temperatures in most of the cases. Thus, accuracy of the measurements is taken as ±0.1 °C.

The phase separation curve is shown in Figure 1. The critical parameters found for this system are T_c = 316.7 K (43.6 °C), V_c = 3330 cm^3 mol^{-1} of boride, and x_c = 0.052 ± 0.003 mole fraction boride. The critical temperature, T_c, is very sensitive to impurities with $\Delta T_c \simeq +40$ °C for salt saturated with water (1.2 wt.% H_2O) and $\Delta T_c \simeq -20$ °C for salt containing 1% methylene chloride. However, measurements of phase separation curves with contaminated salt showed that the other critical parameters including the shape of the curve are not noticeably affected, even at these large impurity levels.

The following equation represents the entire coexistence curve within the experimental uncertainty

$$x = 0.052 + 0.0010(T_c - T) \pm 0.0155(T_c - T)^{1/2} \quad (2)$$

where x is the mole fraction, and the plus and minus signs give the concentrated and dilute branches, respectively.

One interesting feature is the extreme asymmetry of the curve with x_c = 0.052 or volume fraction ϕ_c = 0.135. This is consistent with the corresponding states pattern for ionic systems.[4] It implies much greater solubility of solvents in the salt than the salt solubility in the solvent, and this was observed for various solvents. In this respect, the ionic system is similar to a high polymer.

Another interesting aspect of eq 2 is the final exponent 1/2 which is the critical exponent β. This exponent is found to be near 1/3 for nonionic systems, both liquid–liquid and vapor–liquid, over a wide range of temperature but has been found[5] to be 1/2 for an ionic system somewhat like the present case but with T_c = 414.4 K. Thus, it appears that the shape of the coexistence curve is systematically different for ionic and nonionic systems. The theoretical implications will be explored after the experiments have been extended by other techniques closer to the critical point.

(1) Kraus, C. A. *J. Phys. Chem.* **1954**, *58*, 673.
(2) Ford, W. T.; Hauri, R. J.; Hart, D. J. *J. Org. Chem.* **1973**, *38*, 3916.
(3) Ford, W. T.; Hart, D. J. *J. Phys. Chem.* **1976**, *80*, 1002.
(4) Pitzer, K. S. *J. Phys. Chem.* **1984**, *88*, 2689.
(5) Pitzer, K. S.; de Lima, M. C. P.; Schreiber, D. J. *J. Phys. Chem.* **1985**, *89*, 1854.

0002-7863/88/1510-8723$01.50/0